COMPARISON OF LUNAR ROCKFALLS EVENTS IN DIFFERENT GEOLOGIC SETTINGS USING MINI-RF DATA S. L. Pérez-Cortés[1], A. M. Bramson[1], C. A. Nypaver[2] ,G. W. Patterson[3], A. K. Virkki[4], P. A. Taylor[5], M. C. Nolan[6], M. A. Slade[7]. [1]Purdue University, West Lafayette, IN (sperezco@purdue.edu), [2]The University of Tennessee, Knoxville, [3]JHU-APL, [4]University of Helsinki, [5]NRAO, [6]University of Arizona, [7]NASA JPL/Caltech,.

Introduction: Landslides (e.g., Fig. 1) are a process that affects the surfaces of planetary bodies across the Solar System, including Earth, Mars, the Moon, and Icy Worlds. However, what triggers a landslide to occur, the properties that affect its final geomorphology, and how relevant processes vary across different environments and planetary conditions are still not well understood. Many processes have been proposed to affect the mobility of landslides. Highly mobile "long-runout" landslides have been proposed to be caused by reduced basal friction from the mass sliding over a thin layer of air [1], melted rock [2], or vaporized pore water [3], or from a substrate of low-strength materials such as ice or snow [4–5]. However, long-runout landslides are also observed in dry, granular materials on airless bodies like the Moon [6], which prompted the exploration of mechanisms that do not require involvement of fluids. These proposed dry processes include the mass being supported by dispersive grain stresses from the random movements of individual rock fragments [7] or the collections of fragments organized into an acoustic wave field (i.e., "acoustic fluidization") [8].

Detailed study of the morphologies and environments of mass wasting events on a planetary body can shed light on the contribution of site-specific factors (i.e., substrate material) compared to the role of intrinsic physical processes that govern rock motion (i.e., acoustic fluidization, thermal effects that generate fluidized basal lubrication). Different hypotheses yield different predictions of morphology. For example, in the acoustic fluidization theory, the size of rock fragments in the flow has been suggested to be important in generating low viscosity behavior that leads to long runout distances [9]. Meanwhile, a relationship to latitude would indicate the importance of thermal conditions, and previous studies [10] have investigated how the solar-induced breakdown of rocks could trigger rockfalls on the lunar surface.

This projects aims to build a more complete survey of the distribution of landslides across the lunar surface using Lunar Reconnaissance Orbiter (LRO) data to investigate how these mass wasting events vary across different geologic settings (complex craters, simple craters, tectonic settings) while studying the possible processes that caused them.

Methods: On the Moon, landslide events were previously categorized by [11–12] into rockfalls, rockslides, debris flows, sweeps, creeps, and long runout landslides. Most of these landslide features fell under the category of creeps and rockfalls, with long-runout landslides the rarest. We are currently focused on comparing rockfalls (Fig. 1) and long-runout landslides on the lunar surface in visible and radar datasets to characterize their morphologies and environments. High resolution images from the LRO Camera (LROC) Narrow Angle Cameras (NAC) allows us to map the landslides at a resolution of 0.5 m/pixel. Meanwhile, radar data from LRO's Mini-RF instrument, particularly the circular polarization ratio (CPR) of the received signal, allows us to investigate if there are trends between landslide morphology and various physical properties of the site, such as blockiness at decimeters-to-meters scale (high CPR values in monostatic data) or the presence of an opposition surge (high CPR at low bistatic angles), which can indicate ice in the substrate [13]. We will also look at rock abundances [14] and temperatures [14] derived from Diviner thermal infrared radiometer data.

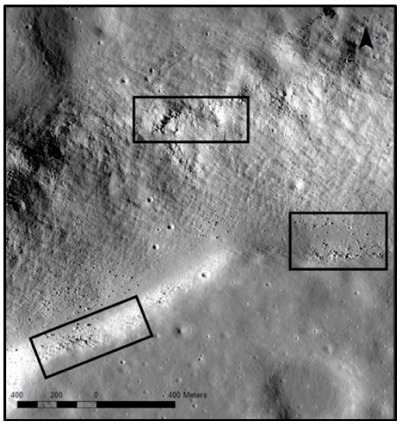

Figure 1: Rockfalls (within black squares) at a tectonic site on the lunar surface (26.23°N, 308.54°E). NAC image: M102493519LE.

Mapping of landslides and geological context. Using [11] as a guide, we are mapping landslides in LROC NAC data with the Java Mission-planning and Analysis for Remote Sensing (JMARS) and ArcGIS software. We are tracing the boundaries of the different events in different locations [11] by looking at the accumulation of sediment and identifying the scarp and talus of landslides or falling of boulders on slopes. We are also making observations at nearby areas and mapping new landslides at each site of interest using NAC images of different illumination conditions at each site of interest. At each site, we are recording the number of the separate events and will keep track of the scale (length and width) of each. For each landslide observed, we are also making observations of its geological context (e.g., if

the locations are on a simple crater, complex crater, in the crater wall or crater floor, a tectonic setting, etc.), and will note the slope it is on, the rock abundance of the area, and the surface temperature environment.

Radar data from Mini-RF. We are using both monostatic (128 ppd) and bistatic (average 100 m/px) radar data from Mini-RF to analyze the CPR in areas with landslides. We are also looking for distinctive patterns in the radar data at the locations of these landslides compared to locations nearby with no landslides. Following previously studies [16], we will also look at same-sense-circular polarization (SC) vs. opposite-sense-circular polarization (OC) data products individually (where CPR = SC/OC). Comparing these datasets of landslides at different sites and in different environments, as well as the sites of landslides to nearby, similar areas with no landslides will help us discern patterns and processes that affect landslide occurrence and morphology.

Preliminary Results: Currently we have mapped more than 150 rockfalls. Preliminary results show CPR values of rockfalls and long-runout landslides at different geologic settings (Fig. 2). Rockfalls at simple and complex craters may exhibit higher CPR values than at tectonic sites, especially at higher latitudes. We will see if this pattern holds after accounting for slope effects.

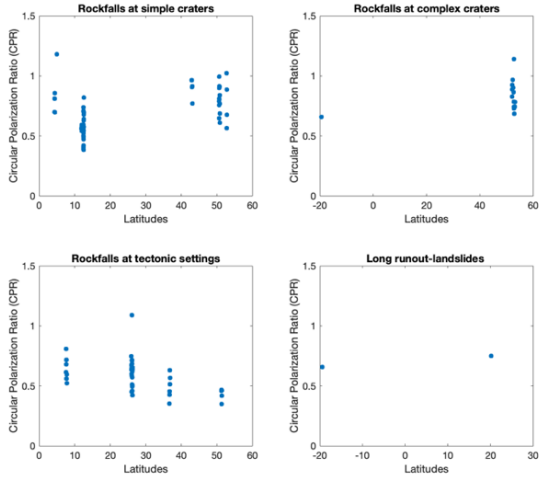

Figure 2: CPR vs. latitude for rockfalls at different geologic settings, as well as for the two long-runout landslides at Mantle Avalanche Valley and the Tsiolkovsky crater. These CPR values are from the monostatic Mini-RF data set.

We have observed finger deposits (described in [17]) on crater walls of simple craters (Figure 3). These finger deposits are fine grained materials sliding down the crater walls and accumulating along with the boulder sized sediments at the crater floor.

Figure 4 shows CPR vs. bistatic angle of rockfalls at three different geologic settings: a complex crater, a simple crater, and a tectonic setting. Currently, we do not see any obvious trends in the bistatic data, although this analysis is preliminary and the sites we have analyzed so far do not include data at low (<6 deg) bistatic angles.

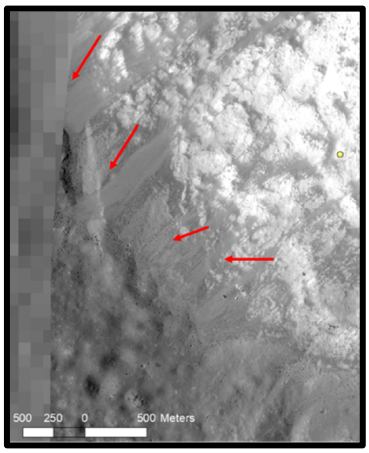

Figure 3: Finger deposits (red arrows) observed in the wall of Marius Crater.

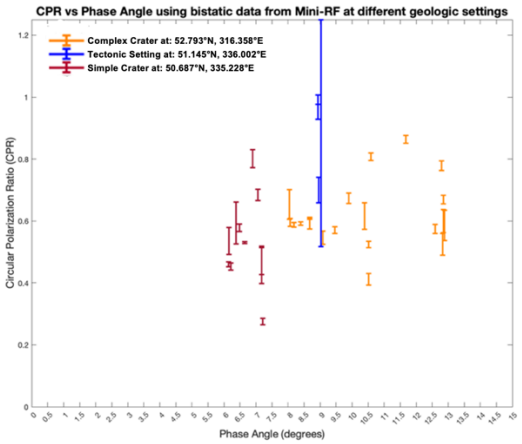

Figure 4: CPR vs. phase (i.e., bistatic) angle of rockfalls at different geologic settings.

Acknowledgments: Mini-RF Monostatic Global Mosaic (128 ppd) is available on the PDS.

References: [1] Shreve (1968) *GSA Special Papers* 108. [2] Erismann (1979) *Rock Mechanics,* 12, 15–46. [3] Goguel (1978) *Developments in Geotechnical Engineering*, 14, 693–705. [4] Aaron & McDougall (2019) *Engineering Geology*, 257. [5] De Blasio (2014) *Geomorphology*, 213, 88–98. [6] Howard (1973) *Science* 180, 1052–1055. [7] Bagnold (1956) *Royal Society*, 249, 235–297. [8] Melosh (1979) *JGR Solid Earth*, 84, 7513–7520. [9] Johnson, Campbell & Melosh (2016) *JGR Earth Surf.*, 121, 881–889. [10] Bickel (2021) *JGR Planets*, 126, E006824. [11] Xiao et al., (2013) *Earth and Plant. Sci. Letters*, *376*, 1–11. [12] Magnarini et al., (2021) *JGR Planets, 126,* 10. [13] Hapke and Blewett (1991) *Nature, 352,* 46–47. [14] Bandfield et al. (2011), JGR 116, E00H02. [14] Williams, J. P. et al. (2017), Icarus 283, 300–325. [16] Virkki & Bhiravarasu (2019) *JGR Planets* 124, 3025–3040. [17] Kumar et al., (2013) *JGR Planets*, 118, 206–223.